J. Fluid Mech. (2006), *vol.* 557, *pp.* 145–165.
doi:10.1017/S0022112006009694 Printed in the United Kingdom

Pressure corrections for the effects of viscosity on the irrotational flow outside Prandtl's boundary layer

By J. WANG AND D. D. JOSEPH

Department of Aerospace Engineering and Mechanics, University of Minnesota, 110 Union St SE, Minneapolis, MN 55455, USA

(Received 13 March 2005 and in revised form 18 November 2005)

This work aims at understanding the viscous effects of the outer potential flow on Prandtl's boundary layer. For a body moving with a constant velocity in an otherwise quiescent liquid, the non-zero viscous dissipation of the outer potential flow gives rise to an additional drag, increasing the drag calculated from the boundary layer alone. The drag is considered in three cases here, on a two-dimensional circular gas bubble in a streaming flow, at the edge of the boundary layer around a rapidly rotating cylinder in a uniform flow, and on an airfoil in a streaming flow. The drag may be computed using the dissipation method or the viscous pressure correction of the irrotational pressure. Such a pressure correction can be induced by the discrepancy between the irrotatinal shear stress and the zero shear stress at a fluid–gas interface, or by the discrepancy between the shear stress evaluated from the boundary-layer solution and that evaluated from the outer potential flow solution at the edge of the boundary layer.

1. Introduction

High-Reynolds-number flows may be approximated by an outer irrotational flow and a boundary layer adjacent to the surface of a body. If the body is a gas bubble with negligible viscosity and density, it is believed that the boundary layer is very thin and weak and a first approximation to the viscous effects to the bubble motion can be obtained from the irrotational flow, without knowledge of the boundary layer. One such approach is the dissipation method, first used by Lamb (1932) to estimate the decay rate of bubble oscillation and free gravity waves. The dissipation is estimated by assuming that the velocity field in the bulk liquid is given by a potential and the contribution to the dissipation from the weak boundary layer is negligible to the first order. Levich (1949) applied the dissipation method to the problem of the drag on a spherical gas bubble rising with velocity U. The drag D is computed by equating the power of the rise DU to the dissipation integral evaluated on the potential flow.

The gas–liquid interface problems addressed by the dissipation method may also be studied by using viscous potential flow with a viscous pressure correction. The pressure correction of the irrotational pressure is induced by the discrepancy between the non-zero irrotational shear stress and the zero-shear-stress condition at the gas–liquid interface. It is generally assumed that this extra pressure can be found in a vorticity boundary layer in the liquid which is so small that it does not contribute to the dissipation integral. Such a theory should lead to appropriate scaling in which small terms in the governing equations could be identified, the size of the

boundary layer, the description of the distribution of velocity, vorticity and especially the distribution of the pressure could be determined. A conventional approach to the problem of the drag on a rising spherical gas bubble, given by Moore (1963) failed to produce an acceptable pressure function for reasons identified by Kang & Leal (1988*a*) who approached the problem of the extra pressure in another way, in which boundary layers are not in evidence. Regarding this approach, Kang & Leal (1988*b*) remark that, 'In the present analysis, we therefore use an alternative method which is equivalent to Lamb's dissipation method, in which we ignore the boundary layer and use the potential-flow solution right up to the boundary, with the effect of viscosity included by adding a viscous pressure correction and the viscous stress term to the normal stress balance, using the inviscid flow solution to estimate their values'. The approach of Kang & Leal is based on an analysis of the nonlinear vorticity equation, and they derived the pressure correction for the spherical bubble in an arbitrary axisymmetric flow field. With this pressure correction, Kang & Leal (1988*a*) computed the drag on a rising spherical gas bubble by direct integration of the traction vector over the bubble surface, and the result is the same as Levich's dissipation result.

Joseph & Wang (2004) presented another way to compute the pressure correction, which is called the viscous correction of viscous potential flow (VCVPF). It is based on the assumption that the motion is irrotational, the shear stress is zero at the interface, the normal stress is computed on the irrotational flow and the extra or corrected pressure can be computed right at the boundary to balance the non-zero irrotational shear stress. This leads to the pressure correction formula

$$\int_A \boldsymbol{u}\cdot\boldsymbol{n}(-p_{\mathrm{v}})\,\mathrm{d}A = \int_A \boldsymbol{u}\cdot\boldsymbol{t}\tau_s\,\mathrm{d}A, \tag{1}$$

which relates the extra pressure p_{v} to the uncompensated irrotational shear stress τ_s. Here, A is the gas–liquid interface; $\boldsymbol{t}$ is the unit tangential vector and $\boldsymbol{n}$ is the unit normal vector on A, pointing from the liquid to the gas. The extra pressure is an additional and important viscous contribution to the normal stress. The extra pressure p_{v} can be expressed on the boundary by a harmonic series. In the case of the rising spherical gas bubble, equation (1) is enough to establish the coefficient of the principal term of the harmonic series; this term, and only this term, enters into the direct computation of the drag by integration of the drag component of the traction vector, and this drag is the same as that computed by the dissipation method. Besides the drag on a spherical rising gas bubble, Joseph & Wang (2004) applied VCVPF to the problems of the drag on a liquid drop rising in another liquid, the drag on an ellipsoidal gas bubble and the decay rate of free gravity waves studied by Lamb (1932). In all the problems, VCVPF gives the same results as the dissipation method. Wang, Joseph & Funada (2005) studied capillary instability using VCVPF; their growth rates are almost indistinguishable from the exact viscous solution.

The work on gas–liquid flows using VCVPF has some interesting possibilities for the analysis of boundary layers on solids. Joseph (2003) discussed the possible consequences of irrotational viscous terms on the conventional Prandtl theory. An additional term $\mu\partial^3\Phi/\partial x^3$, where μ is viscosity and Φ the potential, appears in the boundary-layer equation. This extra term vanishes as the Reynolds number tends to infinity, in the Prandtl limit. Here, following an idea of Joseph, we take an entirely different approach to the effects of irrotational viscous stresses on boundary-layer flow on solid surfaces. We argue that a boundary layer with irrotational motion outside is like a gas bubble because the shear stress vanishes at the edge of the boundary

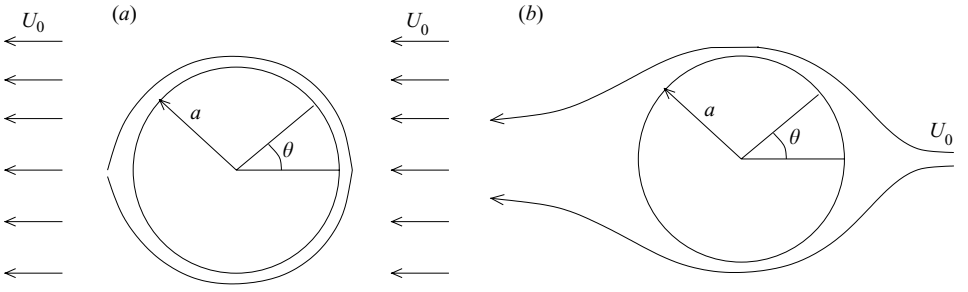

FIGURE 1. The flow past a circular cylinder (*a*) without separation of the boundary layer; (*b*) with separation of the boundary layer.

layer, but the irrotational shear stress does not. This discrepancy induces a pressure correction and an additional drag which can be advertised as due to the viscous dissipation of the irrotational flow. Typically, this extra correction to the drag ought to be relatively small. A much more interesting implication of the extra pressure theory arises from the consideration of the effects of viscosity on the normal stress on a solid boundary which are neglected in Prandtl's theory. It is well known and easily demonstrated that as a consequence of the continuity equation, the viscous normal stress must vanish on a rigid solid. It follows that all the important effects of viscosity on the normal stress are buried in the pressure, but in Prandtl's theory, the pressure is assumed to be the irrotational pressure throughout the boundary layer. VCVPF can give the leading-order effects of viscosity on the pressure at the outer edge of the boundary layer, but not the variation of the pressure inside the boundary layer. An analysis which solves for the pressure in the boundary layer from the governing equations is required to obtain the variation of the pressure inside the boundary layer and eventually the viscous effect on the pressure at the solid wall.

In § 2, we compute the drag on a two-dimensional circular gas bubble using the dissipation method and VCVPF. This problem sets the frame for considerations of the additional drag on the boundary layer around a solid. Figure 1 shows the flow past a circular cylinder. Suppose that there is no separation of the boundary layer (figure 1*a*), the flow is like a uniform flow past a circular gas bubble. The additional drag at the edge of the boundary layer can be computed just like the drag on a gas bubble. Practically, boundary-layer separation occurs (figure 1*b*) and the potential flow solution for the outer flow is not known. One of the methods to suppress separation is to rotate the cylinder rapidly. We compute the additional drag at the edge of the boundary layer of a rapidly rotating cylinder in a uniform flow in § 3. The flow past an airfoil, which can be obtained by conformal transformation from the flow over a rotating cylinder, is the subject of § 4.

2. Pressure corrections for the drag on a circular gas bubble

The drag D per unit length on a stationary circular gas bubble of radius a in a uniform stream $-U_0$ may be obtained using the dissipation method introduced by Levich (1949) to compute the drag on a spherical gas bubble. In our problem, the uniform flow is from right to left (see figure 1). The drag on the bubble is in the uniform flow direction and is negative. The steady rise velocity U_0 of the circular gas bubble in the irrotational flow of a viscous liquid can be obtained from the stationary bubble in a uniform stream by a Galilean transformation. This problem

is a good frame to set the considerations which lead to viscous effects on boundary layers around solid bodies owing to extra pressure generated by the unphysical shear stress as the outer edge of the boundary layer. The solid and its entrained boundary layer can be regarded as a boundary-layer bubble.

The irrotational flow of a viscous liquid over a stationary gas bubble is given by viscous potential flow $\boldsymbol{u}=\nabla\phi$, $\nabla^2\phi=0$. $p=p_{\rm i}$ is the pressure according to Bernoulli's equation; the stress in the liquid is $\boldsymbol{T}=-p_{\rm i}\boldsymbol{1}+2\mu\nabla\otimes\nabla\phi$ where μ is the viscosity.

The velocity potential for the stationary gas bubble is

$$\phi=-U_0 r\left(1+\frac{a^2}{r^2}\right)\cos\theta, \tag{2}$$

and, at $r=a$ we obtain

$$u_r=0, \quad u_\theta=2U_0\sin\theta, \tag{3}$$

and

$$[\tau_{rr},\ \tau_{r\theta}]=-\frac{4\mu U_0}{a}[\cos\theta,\sin\theta] \tag{4}$$

are the normal and shear stresses, respectively, and $p_{\rm i}$ is determined by Bernoulli's equation

$$p_{\rm i}=p_\infty+\tfrac{1}{2}\rho U_0^2(1-4\sin^2\theta). \tag{5}$$

The dissipation $\mathscr{D}$ per unit length of the potential flow may be evaluated using the identity

$$\begin{aligned}\mathscr{D}&\equiv\int_V 2\mu\boldsymbol{D}:\boldsymbol{D}\,{\rm d}V=\int_A \boldsymbol{u}\cdot 2\mu\boldsymbol{D}\cdot\boldsymbol{n}\,{\rm d}A\\&=\int_A -(u_r\tau_{rr}+u_\theta\tau_{r\theta})\,{\rm d}A=8\pi\mu U_0^2,\end{aligned} \tag{6}$$

where $\boldsymbol{D}$ is the symmetric part of the rate of strain tensor, V is the volume occupied by the fluid and A is the boundary of V. The drag due to the dissipation of the potential flow can then be calculated

$$D=\mathscr{D}/(-U_0)=-8\pi\mu U_0. \tag{7}$$

A direct calculation of the drag on the bubble, using viscous potential flow to calculate the stress traction at $r=a$ yields a different result

$$D=\int_A \boldsymbol{e}_x\cdot\boldsymbol{T}\cdot(-\boldsymbol{n})\,{\rm d}A=\int_A[(-p_{\rm i}+\tau_{rr})\boldsymbol{e}_x\cdot\boldsymbol{e}_r+\tau_{r\theta}\boldsymbol{e}_x\cdot\boldsymbol{e}_\theta]\,{\rm d}A=0. \tag{8}$$

This is because the integral of $p_{\rm i}$ vanishes and

$$\int_A \tau_{rr}\boldsymbol{e}_x\cdot\boldsymbol{e}_r\,{\rm d}A=-\int_A \tau_{r\theta}\boldsymbol{e}_x\cdot\boldsymbol{e}_\theta\,{\rm d}A. \tag{9}$$

This result $D=0$ with a non-zero dissipation $8\pi\mu U_0^2$, is a paradox which is even more paradoxical than D'Alembert's.

In an exact formulation of the flow past a circular bubble, without assuming potential flow, and with $\tau_{r\theta}=0$ at $r=a$, we have

$$D=\int_A(-p+\tau_{rr})\boldsymbol{e}_x\cdot\boldsymbol{e}_r\,{\rm d}A. \tag{10}$$

The effects of viscosity can enter this integral through p or τ_{rr}.

We next assume that the non-physical irrotational shear stress $\tau_{r\theta}$ is removed in a boundary layer in which the vorticity is not zero. The thickness δ of the vortical layer is very small at high Reynolds number. The rate of strain in the vortical layer is of the order U_0/a in order that the shear stress be zero; the volume of the vortical layer is of the order $a\delta$ per unit length. Therefore the dissipation per unit length in the vortical layer is of the order $\mu U_0^2\delta/a$, which is negligible compared the dissipation in the bulk volume (6). It is further assumed that the boundary-layer contribution to τ_{rr} is also negligible. It follows then that the direct calculation of drag can agree with the dissipation calculation only if

$$p = p_{\mathrm{i}} + p_{\mathrm{v}}, \tag{11}$$

where p_{v} is the additional contribution to pressure in the vorticity boundary layer. The mechanical energy equation at steady state gives rise to

$$\mathscr{D} \equiv \int_V 2\mu \boldsymbol{D}:\boldsymbol{D}\,\mathrm{d}V = \int_A \boldsymbol{u}\cdot\boldsymbol{T}\cdot\boldsymbol{n}\,\mathrm{d}A. \tag{12}$$

Given the structure described above, we have

$$\mathscr{D} = -\int_A u_r(-p_{\mathrm{v}} + \tau_{rr})\,\mathrm{d}A. \tag{13}$$

Comparing (13) with (6), we can see that (1) holds with $\boldsymbol{n} = -\boldsymbol{e}_r$, $\boldsymbol{t} = -\boldsymbol{e}_\theta$, $\tau_s = \tau_{r\theta}$ in the case of the circular gas bubble.

The extra pressure must be a 2π periodic solution on the circle and can be represented by a Fourier series

$$-p_{\mathrm{v}} = \sum_{k=0}^{\infty}(C_k\cos k\theta + D_k\sin k\theta), \tag{14}$$

Inserting (14) and (4) into (1), we find that

$$-\int_0^{2\pi} U_0\cos\theta\left(C_1\cos\theta + D_1\sin\theta + \sum_{k\neq 1}(C_k\cos k\theta + D_k\sin k\theta)\right)a\,\mathrm{d}\theta = 4\pi\mu U_0^2. \tag{15}$$

The above integration is performed on the surface of the bubble and the vortical layer is not considered. Evaluation of (15) using orthogonality gives

$$C_1 = -4\mu U_0/a. \tag{16}$$

The other coefficients are undetermined. The only term in the Fourier series (14) entering into the direct calculation of the drag is proportional to $\cos\theta$. Hence

$$D = \int_0^{2\pi}(-p_{\mathrm{v}} + \tau_{rr})\boldsymbol{e}_x\cdot\boldsymbol{e}_r\,a\;\mathrm{d}\theta = \int_0^{2\pi}(-p_{\mathrm{v}} + \tau_{rr})a\cos\theta\,\mathrm{d}\theta = -8\pi\mu U_0 \tag{17}$$

is the same D as calculated by the dissipation method in (7).

It is of interest to consider the separate contribution to the drag of $-p_{\mathrm{v}}$ and τ_{rr} in (17)

$$D = D_{p_{\mathrm{v}}} + D_{\tau_{rr}} = -4\pi\mu U_0 - 4\pi\mu U_0 = -8\pi\mu U_0. \tag{18}$$

If somehow the surface of the bubble were made rigid so that the no-slip condition could be realized, then the continuity equation would imply that $D_{\tau_{rr}} = 0$ and $D_{p_{\mathrm{v}}}$ would be the pressure drag on the rigid solid. Moore (1959) calculated the drag on a spherical gas bubble using the viscous normal stress alone and obtained

$D = -8\pi\mu U_0 a$. The Levich drag is $-12\pi\mu U_0 a$, and the difference is the drag $D_{p_v} = -4\pi\mu U_0 a$, which is, in the present mode of imagination, the viscous drag on a rigid sphere due to the viscous irrotational flow.

The existence and asymptotic validity of a boundary layer of the type assumed here and elsewhere have not been established. The details of the size of the layer, the boundary-layer equations, the variation of velocity, vorticity and pressure in the layer have not been given. Kang & Leal (1988*a*) did calculations from the vorticity equation in the case of the drag on a spherical gas bubble. Results indicating a boundary-layer structure of the type described here were obtained, but their results are partial and do not give the details listed above.

The nature of the boundary layer may be determined in the appropriate asymptotic limit more easily in two-dimensions than in three. In the two-dimensional problem, we may obtain an exact solution of the streamfunction equation

$$\frac{1}{r}\frac{\partial\psi}{\partial\theta}\frac{\partial}{\partial r}\nabla^2\psi - \frac{1}{r}\frac{\partial\psi}{\partial r}\frac{\partial}{\partial\theta}\nabla^2\psi = \nu\nabla^4\psi, \tag{19}$$

where

$$\nabla^2\psi = \frac{1}{r}\frac{\partial}{\partial r}\left(r\frac{\partial\psi}{\partial r}\right) + \frac{1}{r^2}\frac{\partial^2\psi}{\partial\theta^2},$$

in the region outside the circle subject to the conditions that

$$\boldsymbol{u} = -\boldsymbol{e}_x U_0 \quad \text{at } \infty, \tag{20}$$

and

$$u_r = 0, \quad \tau_{r\theta} = 0 \quad \text{at } r = a. \tag{21}$$

This problem is well posed; it is like the flow over a stationary solid cylinder except that the no-slip condition on the tangential velocity on the stationary solid circle is replaced by a zero-shear-stress condition on a circular bubble.

The solution of (19), (20) and (21) determines a streamfunction $\psi(r, \theta)$. Once this function is determined, the pressure may be determined from the equations of motion and the pressure correction can be obtained.

3. A rotating cylinder in a uniform stream

The potential flow over a rotating cylinder in a uniform stream plays an important role in classical airfoil theory in which the flow and airfoil shape is obtained by conformal transformation, and the Kutta condition suppressing separation at the trailing edge is obtained by adjusting the ratio of the rotational speed to the streaming speed.

We study the extra pressure contribution to the drag at the outer edge of Prandtl's boundary layer on a solid cylinder rotating so fast that the separation of the boundary layer is suppressed. We compare the analysis of the extra pressure associated with the viscous dissipation of the irrotational flow outside the boundary layer with a numerical solution of the unapproximated equations for values as close to the appropriate asymptotic values as the numerical solution will allow. In our problem, the uniform flow is from right to left (see figure 1) and the cylinder rotates counterclockwise. The lift on the cylinder points upward and is positive. The drag on the cylinder is negative if it is in the uniform flow direction; the drag is positive if it is opposite to the uniform flow direction.

Our work here is motivated by the desire to understand the dynamical effect of the fact that the viscous dissipation of the irrotational flow outside Prandtl's boundary layer is not zero and that the viscous effects on the normal stress on a solid are due only to the pressure and at finite-Reynolds number, no matter how large, there will be a viscous effect on the pressure, not given in Prandtl's theory.

3.1. *Dissipation calculation*

We consider the uniform flow $-U_0$ past a fixed circular cylinder with circulation Γ. Suppose no separation of the boundary layer occurs, the flow outside the boundary layer is given by the potential

$$\phi = -U_0 r\left(1+\frac{a^2}{r^2}\right)\cos\theta + \frac{\Gamma\theta}{2\pi}. \tag{22}$$

The velocity and stress at the surface of the cylinder can be evaluated using (22):

$$u_r = 0, \quad u_\theta = 2U_0\sin\theta + \frac{\Gamma}{2\pi a}, \tag{23}$$

$$\tau_{rr} = -4\mu U_0\cos\theta/a, \quad \tau_{r\theta} = -4\mu U_0\sin\theta/a - \mu\Gamma/(\pi a^2). \tag{24}$$

The dissipation $\mathscr{D}$ of the potential flow can be evaluated:

$$\mathscr{D} = -\int_A (u_r\tau_{rr} + u_\theta\tau_{r\theta})\,\mathrm{d}A = 8\pi\mu U_0^2 + \frac{\mu\Gamma^2}{\pi a^2}. \tag{25}$$

The dissipation is equal to the sum of the dissipation of an irrotational purely rotary flow and a streaming flow past a fixed cylinder; the cross-terms in $u_\theta\tau_{r\theta}$ do not appear in the dissipation expression because they integrate to zero. The dissipation of the potential flow should be equal to the power of the drag D and the torque T

$$D(-U_0) + T\frac{\Gamma}{2\pi a^2} = \mathscr{D}. \tag{26}$$

Ackeret (1952) computed the same dissipation for the problem under consideration. He did not consider the torque and equated the dissipation to the power of the drag alone and obtained

$$D = \mathscr{D}/(-U_0) = -8\pi\mu U_0 - \frac{\mu\Gamma^2}{\pi a^2 U_0}. \tag{27}$$

Ackeret argued that it is worth considering the potential flow solution if the viscous liquid is allowed to slip at solid boundaries. He did not mention gas bubbles, liquid–gas flows, the additional drag or the relation of his solution to unphysical irrotational shear stress at the edge of the boundary layer.

We argue that the additional drag cannot be computed from (26) with the torque T undetermined. We will obtain the additional drag in § 3.3 by computing the pressure correction p_v, following the method laid down in our calculation of p_v in the case of a circular gas bubble.

3.2. *Boundary-layer analysis*

Glauert (1957) carried out a boundary-layer analysis of the flow past a rotating cylinder. He assumed that the ratio

$$\alpha = 2U_0/Q, \tag{28}$$

where U_0 is magnitude of the uniform stream velocity and Q is the circulatory velocity of the flow at the outer edge of the boundary layer, is smaller than unity and

separation is suppressed. He obtained a solution of the boundary-layer equations in the form of a power series in α, and deduced the ratio Q/q, where q is the cylinder's peripheral velocity. The term q is related to the angular velocity Ω of the cylinder by $q = \Omega a$. Glauert's solution suggests that Q is approximately equal to q for large values of q; it follows that

$$\alpha \to 2U_0/q = \frac{2}{q/U_0} \quad \text{as} \quad q \to \infty. \tag{29}$$

Glauert used Prandtl's boundary-layer theory in which the irrotational pressure of the outer flow is imposed on the solid wall through the boundary layer. Assuming that the boundary-layer thickness is negligible compared to the cylinder radius, Glauert used the boundary-layer equations for steady two-dimensional flows:

$$\frac{\partial u}{\partial x} + \frac{\partial v}{\partial y} = 0, \tag{30}$$

$$u\frac{\partial u}{\partial x} + v\frac{\partial u}{\partial y} = U\frac{\mathrm{d}U}{\mathrm{d}x} + \nu\frac{\partial^2 u}{\partial y^2}, \tag{31}$$

where U is the irrotational velocity at the edge of the boundary layer. x is measured round the cylinder circumference and y normal to it. Glauert chose $x = 0$ to be the point at which the surface moves in the same direction as the uniform stream (the top of the cylinder). We will follow his choice here. Let φ represent the polar angle measured from the point $x = 0$, then $\varphi = x/a$. Glauert obtained the following solutions

$$u = Q(1 + \alpha f_1'(y)\mathrm{e}^{\mathrm{i}\varphi} + \alpha^2[f_2'(y)\mathrm{e}^{2\mathrm{i}\varphi} + g_2'(y)] + \cdots), \tag{32}$$

$$v = -Q\left[\frac{\mathrm{i}}{a}\alpha f_1(y)\mathrm{e}^{\mathrm{i}\varphi} + \frac{2\mathrm{i}}{a}\alpha^2 f_2(y)\mathrm{e}^{2\mathrm{i}\varphi} + \cdots\right], \tag{33}$$

$$\frac{\partial u}{\partial y} = Q(\alpha f_1''\mathrm{e}^{\mathrm{i}\varphi} + \alpha^2[f_2''(y)\mathrm{e}^{2\mathrm{i}\varphi} + g_2''(y)] + \cdots), \tag{34}$$

where $f_1(y)$, $f_2(y)$ and $g_2(y)$ are functions of y and were determined by Glauert. Because $f_1'(0) = f_2'(0) = 0$ and $g_2'(0) > 0$ given by Glauert's solution, the velocity at the surface of the cylinder can be obtained from (32):

$$q = Q(1 + \alpha^2 g_2'(0) + \cdots), \tag{35}$$

which shows that $Q < q$. Since the shear stress at the cylinder surface is given by $\mu(\partial u/\partial y)_{y=0}$, it can be inferred from (34) that the shear stress is zero at the cylinder surface when α is zero. In other words, when there is no streaming flow, but only viscous irrotational rotary flow, Glauert's solution suggests that the shear stress at the cylinder surface is zero. However, the real shear stress is $-2\mu q/a$.

The reason for this discrepancy is that the irrotational rotary flow component is not considered in Glauert's solution, which is an approximation consistent with the assumption that δ/a is negligible compared to 1. Thus, the shear stress induced by the rotary flow is ignored. The irrotational rotary component of the velocity inside the boundary layer can be written as

$$u_{p\varphi} = Q\frac{a + \delta}{r}, \tag{36}$$

where δ is the thickness of the boundary layer. We propose a simple modification of Glauert's solution

$$u_\varphi = u_{p\varphi} + u_b = Q\left(\frac{a+\delta}{r} + \alpha f_1'(y)\mathrm{e}^{\mathrm{i}\varphi} + \alpha^2[f_2'(y)\mathrm{e}^{2\mathrm{i}\varphi} + g_2'(y)] + \cdots\right), \tag{37}$$

$$u_r = v_b = -Q\left[\frac{\mathrm{i}}{a}\alpha f_1(y)\mathrm{e}^{\mathrm{i}\varphi} + \frac{2\mathrm{i}}{a}\alpha^2 f_2(y)\mathrm{e}^{2\mathrm{i}\varphi} + \cdots\right]. \tag{38}$$

$f_1(y)$, $f_2(y)$, $g_2(y)\cdots$ are solutions of boundary-layer equations (30) and (31), which are based on the assumption that δ/a is negligible compared to 1. Under the same assumption, $(a+\delta)/r \approx 1$ inside the boundary layer and (37) reduces to Glauert's solution (32). Thus, it appears that the $(a+\delta)/r$ term is not consistent with the solutions of $f_1(y)$, $f_2(y)$ and $g_2(y)$. However, (37) is a simple modification to address the defect of ignoring the irrotational rotary component of the flow inside the boundary layer. We will show that the modified Glauert's solution is in better agreement with numerical simulation data than Glauert's solution.

In the companion paper, Wang & Joseph (2006) carried out a new boundary-layer analysis for the flow past a rotating cylinder, in which the inconsistency mentioned above is resolved. The velocity inside the boundary layer is decomposed into a viscous irrotational purely rotary flow and a boundary-layer flow. A new set of equations for the boundary-layer flow is obtained after inserting this decomposition of the velocity into the governing equations. Wang & Joseph do not ignore the terms in the order of δ/a or higher and solve the new set of equations following Glauert's method, i.e. to expand the solution as a power series of $\alpha = 2U_0/Q$. Comparisons with the numerical simulation data of Padrino & Joseph (2006) show that the solution by Wang & Joseph (2006) is an improvement of Glauert's solution. Another possible way to improve Glauert's solution is the higher-order boundary-layer theory based on the method of matched asymptotic expansions (Van Dyke 1962, 1969; Maslen 1963). The rotary-flow component may be taken into account in the second-order corrections of the boundary-layer analysis. However, the higher-order boundary-layer theory has not been applied to the flow past a rotating cylinder and a comparison with our simple modification is not available.

A key problem in the boundary-layer analysis is to determine the circulatory velocity Q when given the cylinder rotational speed q. At $y=0$ ($r=a$), (37) gives rise to

$$\begin{aligned} q &= Q\left[\frac{a+\delta}{a} + \alpha^2 g_2'(0) + \alpha^4 h_4'(0)\right] \\ &= Q\left[1 + \frac{\delta}{a} + 3\left(\frac{U_0}{Q}\right)^2 - 5.76\left(\frac{U_0}{Q}\right)^4\right], \end{aligned} \tag{39}$$

where Glauert's solutions for g_2 and h_4 have been used and the terms of the order of α^5 or higher are ignored. We invert (39) to obtain the expression for Q in terms of q

$$\frac{Q}{q} = \frac{1}{1+\delta/a} - 3\left(\frac{U_0}{q}\right)^2 - 3.23\left(1 - 0.803\frac{\delta}{a}\right)\left(\frac{U_0}{q}\right)^4. \tag{40}$$

If δ/a is ignored, (40) reduces to

$$\frac{Q}{q} = 1 - 3\left(\frac{U_0}{q}\right)^2 - 3.23\left(\frac{U_0}{q}\right)^4, \tag{41}$$

which is the same as Glauert's result. When $U_0 = 0$, there is only irrotational purely rotary flow and the boundary layer does not exist. Thus, $\delta = 0$ and (40) indicates $Q = q$.

We calculate the shear stress at the cylinder surface. The contribution from the irrotational purely rotary flow is

$$\mu\left(\frac{\partial u_{p\varphi}}{\partial r} - \frac{u_{p\varphi}}{r}\right) = -2\mu Q\frac{a+\delta}{a^2} \quad \text{at } r = a,$$

which is added to Glauert's shear stress to obtain the total shear stress

$$\tau_{r\varphi} = \mu Q\left[-2\frac{a+\delta}{a^2} + \alpha f_1''(0)\mathrm{e}^{\mathrm{i}\varphi} + \alpha^2[f_2''(0)\mathrm{e}^{2\mathrm{i}\varphi} + g_2''(0)] + \cdots\right]. \tag{42}$$

The torque T on the cylinder is given by

$$T = -a^2\int_0^{2\pi}\tau_{r\varphi}\mathrm{d}\varphi. \tag{43}$$

Only terms independent of φ in (42) contribute to (43) and we obtain

$$T = 8\pi\rho U_0^2\frac{a(a+\delta)}{Re}\frac{Q}{U_0} + 4\pi\rho U_0^2\frac{a^2}{\sqrt{Re}}\left[\left(\frac{U_0}{Q}\right)^{1/2} - 2.022\left(\frac{U_0}{Q}\right)^{5/2} + \cdots\right], \tag{44}$$

$$C_T = \frac{T}{2\rho U_0^2 a^2} = 4\pi\left(1+\frac{\delta}{a}\right)\frac{1}{Re}\frac{Q}{U_0} + \frac{2\pi}{\sqrt{Re}}\left[\left(\frac{U_0}{Q}\right)^{1/2} - 2.022\left(\frac{U_0}{Q}\right)^{5/2} + \cdots\right], \tag{45}$$

where C_T is the torque coefficient and

$$Re = 2U_0 a/\nu \tag{46}$$

is the Reynolds number based on U_0. The first term on the right-hand side of (44) is the torque induced by the rotary-flow component and is of the order of $1/Re$; the second term is the torque given by Glauert and is of the order of $1/\sqrt{Re}$. When $Re \to \infty$, the term by Glauert is the dominant one. However, when Re is finite and Q/U_0 is large, the first term can be more significant than the second one. When $U_0 = 0$, the torque is equal to $T = 4\pi\mu qa$, which is the torque on the cylinder when there is only the viscous irrotational purely rotary flow.

Glauert cited Reid's (1924) experimental result about the torque

$$T = 20\pi\rho U_0^2\frac{a^2}{\sqrt{Re}}, \tag{47}$$

which was measured for $q = U_0$. Glauert noted that Reid's torque was far above the value given by him and remarked about this discrepancy, 'but it is doubtful if it has much accuracy or relevance, in view of the experimental imperfections and also the separation occurring at this low rotational speed'. We will compare our torque expression to the results of numerical simulation in which the rotational speed is high and separation is suppressed.

The lift and drag on the cylinder are given by the pressure and shear stress at the wall. The pressure in Glauert's solution is a constant across the boundary layer and is equal to the irrotational pressure at the outer edge of the boundary layer; it does not give drag, and the pressure lift can be computed using the classical lift coefficient formula in aerodynamics:

$$C_{L_p} = \frac{\rho U_0\Gamma}{\rho U_0^2 a} = \frac{2\pi Q}{U_0}. \tag{48}$$

In our simple modification of Glauert's solution, we add the irrotational rotary flow component $u_{p\varphi}$ to the velocity and the pressure induced by $u_{p\varphi}$ is

$$p_p = p_{pc} - \tfrac{1}{2}\rho u_{p\varphi}^2 = p_{pc} - \tfrac{1}{2}\rho \frac{(a+\delta)^2}{r^2} Q^2, \tag{49}$$

where p_{pc} is a constant for the pressure. As an approximation, we assume that the total pressure is obtained by a simple addition of p_p and the pressure given by Glauert. On the cylinder surface $r = a$, p_p is independent of θ and does not contribute to the lift. Therefore the pressure lift expression (48) still holds. After inserting (40) into (48), we obtain

$$C_{L_p} = 2\pi \frac{q}{U_0}\left[\frac{1}{1+\delta/a} - 3\left(\frac{U_0}{q}\right)^2 - 3.23\left(1 - 0.803\frac{\delta}{a}\right)\left(\frac{U_0}{q}\right)^4\right]. \tag{50}$$

Since our Q, (40), is smaller than Glauert's result, (41), our pressure lift is smaller than Glauert's. Glauert did not consider the friction drag and lift, but they can be computed easily from his solution:

$$C_{D_f} = \frac{D_f}{\rho U_0^2 a} = -\frac{2\pi}{\sqrt{Re}}\sqrt{\frac{Q}{U_0}}, \qquad C_{L_f} = \frac{L_f}{\rho U_0^2 a} = \frac{2\pi}{\sqrt{Re}}\sqrt{\frac{Q}{U_0}}. \tag{51}$$

Our simple modification changes the shear stress at the wall only by a constant, thus the expressions for the friction drag and lift do not change, but their values change due to Q.

We compare our simple modification of Glauert's solution, the results of numerical simulation from the companion paper Padrino & Joseph (2006) and Glauert's solution in table 1. Six cases, $(Re,\ q/U_0) = (200,\ 4)$, (200, 5), (400, 4), (400, 5), (400, 6) and (1000, 3), are considered. Though the boundary-layer thickness δ/a is not required in Glauert's solution, it must be prescribed in our simple modification. We choose an effective boundary-layer thickness $\delta/a = \delta_L/a$ which is determined by matching C_{L_p} computed from our simple modification (50) to the results of numerical simulation. Table 1 shows that $\delta_L/a \ll 1$, δ_L/a decreases with increasing Re at a fixed q/U_0, and δ_L/a generally decreases with increasing q/U_0, because the rotary flow suppresses the boundary layer. The torque coefficient is not sensitive to the choice of δ/a as long as $\delta/a \ll 1$, which can be seen from (45) and (40). The pressure lift and torque in numerical simulation are obtained by integration at the cylinder surface. The values of $\alpha = 2U_0/Q$ are listed for Glauert's solution and our simple modification for each pair of Re and q/U_0. For $(Re,\ q/U_0) = (1000,\ 3)$, $\alpha > 1$ for both our simple modification and Glauert's solution. These solutions are not expected to converge to the true results. A comparison of the solutions with $\alpha < 1$ shows that the values of C_{L_p} from our simple modification and numerical simulation are smaller than those from Glauert's solution; the values of the torque from our simple modification are much closer to the numerical results than those from Glauert's solution.

If the results of numerical simulation are not available, our analysis cannot provide the value of δ/a. Then Glauert's pressure lift may be taken as a reasonable approximation, and the torque coefficient may be computed from (45) with $\delta/a = 0$. Since the torque coefficient is not sensitive to the choice of δ/a, it still improves Glauert's solution of the torque substantially.

Solution	Re	q/U_0	δ_L/a	α	C_{L_p}	C_T
Glauert's solution	200	4	–	0.625	20.102	0.215
Modified Glauert's solution	200	4	0.145	0.741	16.961	0.390
Numerical simulation	200	4	–	–	16.961	0.453
Glauert's solution	200	5	–	0.457	27.483	0.195
Modified Glauert's solution	200	5	0.0434	0.480	26.183	0.465
Numerical simulation	200	5	–	–	26.183	0.514
Glauert's solution	400	4	–	0.625	20.102	0.152
Modified Glauert's solution	400	4	0.112	0.714	17.609	0.237
Numerical simulation	400	4	–	–	17.609	0.275
Glauert's solution	400	5	–	0.457	27.483	0.138
Modified Glauert's solution	400	5	0.0354	0.476	26.415	0.272
Numerical simulation	400	5	–	–	26.415	0.297
Glauert's solution	400	6	–	0.365	34.463	0.126
Modified Glauert's solution	400	6	0.0380	0.380	33.087	0.299
Numerical simulation	400	6	–	–	33.087	0.316
Glauert's solution	1000	3	–	1.064	11.812	0.108
Modified Glauert's solution	1000	3	0.0837	1.207	10.409	0.0632
Numerical simulation	1000	3	–	–	10.409	0.118

TABLE 1. Comparison of the coefficients for the pressure lift and torque on the cylinder obtained from Glauert's solution, the simple modification of Glauert's solution and numerical simulation. In the simple modification of Glauert's solution, we use an effective boundary-layer thickness δ_L/a, which is determined by matching C_{L_p} computed from our simple modificatio, (50), to the results of numerical simulation. For $(Re,\ q/U_0) = (1000,\ 3)$, $\alpha > 1$ for both our simple modification and Glauert's solution. These solutions are not expected to converge to the true results.

3.3. *Pressure correction and the additional drag*

We consider the pressure correction at the outer edge of the boundary layer and the additional drag induced by it. The shear stress at the outer edge of the boundary layer can be computed in two ways: from the outside potential flow or from the boundary-layer solution. If we consider a rotating cylinder with its entrained boundary layer moving with U_0 in a liquid, the potential flow outside $r = a + \delta$ has the following velocity

$$u_\theta = U_0 \frac{(a+\delta)^2}{r^2} \sin\theta + Q\frac{a+\delta}{r}, \quad u_r = U_0 \frac{(a+\delta)^2}{r^2}\cos\theta. \tag{52}$$

The irrotational shear stress at $r = a + \delta$ is

$$\tau_{r\theta} = -\mu\left(\frac{4U_0 \sin\theta}{a+\delta} + \frac{2Q}{a+\delta}\right). \tag{53}$$

The shear stress from the boundary-layer analysis is

$$\begin{aligned}\tau_{r\theta} &= \mu\left(\frac{\partial u_{p\varphi}}{\partial r} - \frac{u_{p\varphi}}{r} + \frac{\partial u_b}{\partial y} + \frac{\partial v_b}{\partial x}\right) \\ &= \mu\left[-2Q\frac{a+\delta}{r^2} + Q\alpha f_1''(y)\sin\theta + \cdots + Q\frac{\alpha}{a^2} f_1 \sin\theta + \cdots\right].\end{aligned} \tag{54}$$

Glauert's solution gives $f_1''(\delta) \approx 0$ and $f_1(\delta) \sim O(\delta)$, which is negligible. Thus the shear stress at $r = a + \delta$ from the boundary-layer solution is approximately

$$\tau_{r\theta} \approx -\mu \frac{2Q}{a+\delta}. \tag{55}$$

Comparing (53) with (55), we can see that the shear stress is not continuous and the discrepancy is

$$\tau_{r\theta}^{d} = -\mu \frac{4U_0 \sin\theta}{a+\delta}. \tag{56}$$

This shear stress discrepancy induces extra vorticity at the outer edge of the boundary layer and a pressure correction. The power of the pressure correction is equal to the power of the shear stress discrepancy

$$-\int_0^{2\pi} u_r(-p_{\mathrm{v}})(a+\delta)\,\mathrm{d}\theta = -\int_0^{2\pi} u_\theta \tau_{r\theta}^{d}(a+\delta)\,\mathrm{d}\theta = 4\pi\mu U_0^2. \tag{57}$$

Again we expand the pressure correction as a Fourier series (14) and insert it into (57)

$$-\int_0^{2\pi} U_0 \cos\theta \left(C_1 \cos\theta + D_1 \sin\theta + \sum_{k\neq 1} (C_k \cos k\theta + D_k \sin k\theta) \right)(a+\delta)\,\mathrm{d}\theta = 4\pi\mu U_0^2, \tag{58}$$

which gives rise to

$$-C_1 = \frac{4\mu U_0}{a+\delta},$$

$$p_{\mathrm{v}} = \frac{4\mu U_0}{a+\delta}\cos\theta - D_1 \sin\theta - \sum_{k\neq 1}(C_k \cos k\theta + D_k \sin k\theta). \tag{59}$$

We evaluate the additional drag by direct integration of the traction vector at the outer edge of the boundary layer

$$D = \int_0^{2\pi} [(-p_{\mathrm{i}} - p_{\mathrm{v}} + \tau_{rr})\boldsymbol{e}_x \cdot \boldsymbol{e}_r + \tau_{r\theta}\boldsymbol{e}_x \cdot \boldsymbol{e}_\theta](a+\delta)\,\mathrm{d}\theta, \tag{60}$$

where τ_{rr} is the viscous normal stress evaluated on the potential flow velocity, (52), $\tau_{r\theta}$ is the shear stress, (55), evaluated using the boundary-layer solution. The above choices are made because τ_{rr} is essentially continuous at the outer edge of the boundary layer, but $\tau_{r\theta}$ is not; we choose $\tau_{r\theta}$ from the boundary-layer solution and this is analogous to using zero shear stress at a gas–liquid interface. The irrotational pressure p_{i} does not contribute to the drag and we may write (60) as

$$\begin{aligned} D &= \int_0^{2\pi} (-p_{\mathrm{v}})\cos\theta(a+\delta)\,\mathrm{d}\theta + \int_0^{2\pi} \tau_{rr}\cos\theta(a+\delta)\,\mathrm{d}\theta - \int_0^{2\pi} \tau_{r\theta}\sin\theta(a+\delta)\,\mathrm{d}\theta \\ &= -4\pi\mu U_0 - 4\pi\mu U_0 - 0 = -8\pi\mu U_0, \end{aligned} \tag{61}$$

which is the same as the drag on a circular gas bubble, (17). Our additional drag, (61), is much smaller than that, computed by Ackeret (1952) (27), when the rotational velocity is much larger than the streaming velocity. Equation (61) indicates that the additional drag depends only on the forward speed U_0 and not on the spinning speed q. The additional drag should be the drag evaluated at the outer edge of the boundary layer, but the boundary-layer thickness does not affect the additional drag since δ/a does not appear in (61).

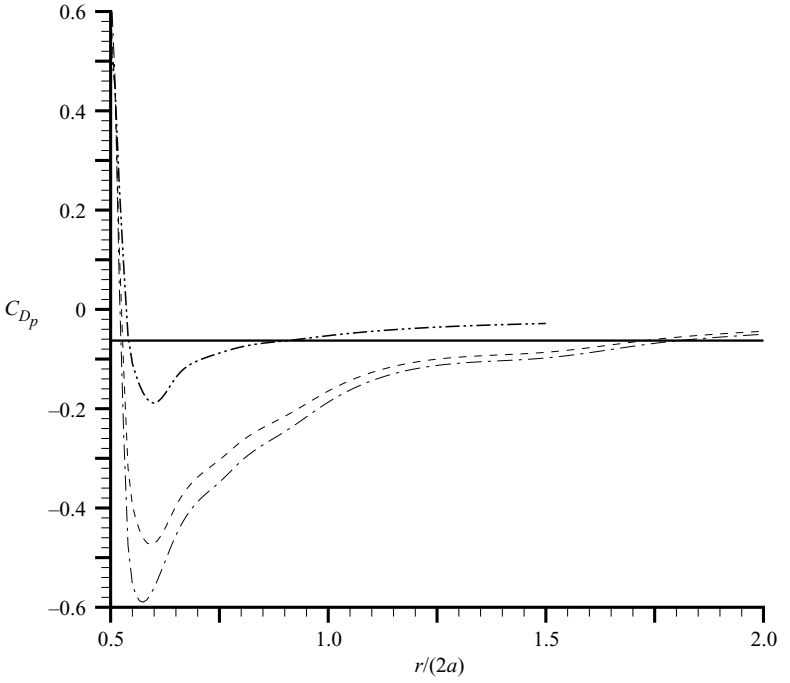

FIGURE 2. The pressure drag coefficient C_{D_p} at different radial position $r/(2a)$ computed from numerical simulation (63) for $Re = 400$: dash-double-dotted line, $q/U_0 = 4$; dashed line, $q/U_0 = 5$; dash-dotted line, $q/U_0 = 6$. The solid straight line gives C_{D_p} computed from (62) for $Re = 400$. Each curve for $C_{D_p}(r)$ has two intersections with the straight line, at which C_{D_p} given by (62) is equal to C_{D_p} computed from numerical simulation at $r = a + \delta$.

If we only consider the additional drag due to the pressure, we obtain

$$D_p = -4\pi\mu U_0, \quad C_{D_p} = \frac{D_p}{\rho U_0^2 a} = -\frac{8\pi}{Re}, \tag{62}$$

which should be compared to C_{D_p} computed from numerical simulation at the outer edge of the boundary layer. However, in practice, the vorticity extends to infinity and a clear-cut boundary-layer edge does not exist. To address this difficulty, we present C_{D_p} computed from numerical simulation at different values of r

$$C_{D_p}(r) = \frac{1}{\rho U_0^2 a} \int_0^{2\pi} (-p)\boldsymbol{e}_x \cdot \boldsymbol{e}_r \, r \, \mathrm{d}\theta, \tag{63}$$

and compare to C_{D_p} from (62). As an example, we plot $C_{D_p}(r)$ from numerical simulation for $Re = 400$ and $q/U_0 = 4$, 5 and 6 in figure 2; the straight line gives C_{D_p} computed from (62) for $Re = 400$. Note that the results of numerical simulation depend on q/U_0, but equation (62) does not. Each curve for $C_{D_p}(r)$ has two intersections with the straight line, the one close to the wall denoted by δ_{D1}/a and the other one far way from the wall denoted by δ_{D2}/a. In table 2, we give the values of δ_{D1}/a and δ_{D2}/a for $(Re, q/U_0) = (200, 4)$, $(200, 5)$, $(400, 4)$, $(400, 5)$, $(400, 6)$ and $(1000, 3)$. The vorticity field in the whole domain was computed in numerical simulation. The magnitude of the vorticity on the circle with the radius $r = a + \delta_{D1}$ or $r = a + \delta_{D2}$ was estimated from the numerical data of Padrino & Joseph (2006) and expressed as a certain percentage of the maximum magnitude of the vorticity field. This percentage

Re	q/U_0	C_{D_p}	δ_{D1}/a	Vorticity (%)	δ_{D2}/a	Vorticity (%)
200	4	−0.126	0.161	13.1	0.594	0.913
200	5	−0.126	0.0838	14.6	2.03	0.00455
400	4	−0.0628	0.0835	18.1	0.811	0.418
400	5	−0.0628	0.0553	20.8	2.46	0.00340
400	6	−0.0628	0.0473	20.7	2.65	0.00365
1000	3	−0.0251	0.0552	20.4	1.56	0.0139

TABLE 2. The values of δ_{D1}/a and δ_{D2}/a at which C_{D_p} given by (62) is equal to C_{D_p} computed from numerical simulation (63). The magnitude of the vorticity on the circle with the radius $r = a + \delta_{D1}$ or $r = a + \delta_{D2}$ was estimated from the numerical data of Padrino & Joseph (2006) and expressed as a certain percentage of the maximum magnitude of the vorticity field. This percentage is between 12.6 % and 20.4 % at $r = a + \delta_{D1}$ and is between 0.003 % and 0.913 % at $r = a + \delta_{D2}$.

Re	q/U_0	δ_{D1}/a	α	C_{L_p}	C_T
200	4	0.161	0.754	16.659	0.388
200	5	0.0838	0.501	25.065	0.466
400	4	0.0835	0.691	18.188	0.239
400	5	0.0553	0.486	25.845	0.273
400	6	0.0473	0.384	32.765	0.299
1000	3	0.0552	1.157	10.862	0.0718

TABLE 3. The calculation of C_{L_p}, (50), and C_T, (45), on the cylinder using δ_{D1}/a determined by matching C_{D_p} as an effective boundary-layer thickness. The results are in fair agreement with the numerical data shown in table 1. This demonstrates that δ_{D1}/a can be used not only as an effective boundary-layer thickness for C_{D_p}, but also for C_{L_p} and C_T.

is between 12.6 % and 20.4 % at $r = a + \delta_{D1}$ and is between 0.003 % and 0.913 % at $r = a + \delta_{D2}$. This percentage is 20.6 % at $r = a + \delta_{D1}$ for $(Re,\ q/U_0) = (400,\ 6)$, which indicates that roughly speaking, the vorticity magnitude at a radial position $r > a + \delta_{D1}$ is less than 20.6 % of the maximum vorticity magnitude. The reason is that the vorticity magnitude generally decreases as r increases. When $r > a + \delta_{D2}$, the vorticity is almost negligible.

A comparison of tables 1 and 2 shows that δ_{D1}/a is close to the effective boundary-layer thickness δ_L/a determined by matching C_{L_p}. When we insert δ_{D1}/a into the expressions for C_{L_p} and C_T on the cylinder, (50) and (45) respectively, the results are in fair agreement with the numerical simulation and are better than Glauert's solutions (see tables 3 and 1). Thus, δ_{D1}/a can be used not only as an effective boundary-layer thickness for C_{D_p}, but also for C_{L_p} and C_T. This result shows that one effective boundary-layer thickness for both the VCVPF calculation and the simple modification of Glauert's solution exists.

Figure 2 shows that C_{D_p} changes significantly with r near the wall; C_{D_p} reaches its minimum then increases; the magnitude of C_{D_p} approaches zero as r increases to infinity. In the region near the second intersection $r = a + \delta_{D2}$, the C_{D_p} curve is rather flat and the straight line given by (62) is a reasonable approximation to the numerical results. This region may be viewed as a transition region from the inner flow where the vorticity is important to the outer flow where the vorticity is negligible. The VCVPF calculation cannot predict variation of C_{D_p} near the wall.

The term $D_1 \sin\theta$ in the pressure correction should give rise to an extra lift force in addition to the contribution from the irrotational pressure. However, D_1 is not

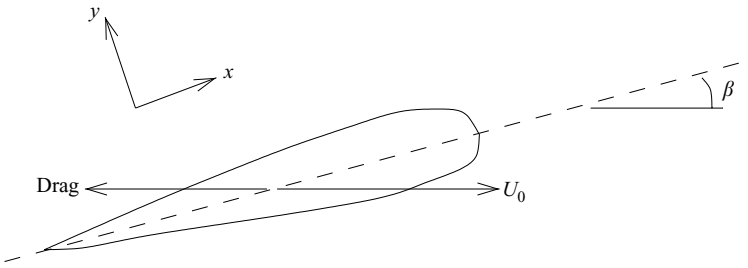

FIGURE 3. A symmetrical airfoil moving in a liquid at an angle of attack β with a constant velocity U_0. The additional drag on the airfoil computed using the dissipation method is opposite to the moving direction of the airfoil and is defined as negative.

determined in the VCVPF calculation. In Wang & Joseph's (2006) new boundary-layer analysis, the pressure is not assumed to be a constant across the boundary layer and it is solved from the governing equations. Wang & Joseph determined the terms proportional to $\sin\theta$, $\cos\theta$, $\sin 2\theta$ and $\cos 2\theta$ up to $O(\alpha^2)$.

4. The additional drag on an airfoil by the dissipation method

We consider a symmetrical Joukowski airfoil moving in a liquid at an angle of attack β with a constant velocity U_0 (figure 3). The airfoil is obtained by the Joukowski transformation

$$z = \zeta + \frac{c^2}{\zeta}, \tag{64}$$

in conjunction with a circle in the ζ-plane. The radius a of the circle is slightly larger than the transformation coefficient c,

$$a = c + m = c(1 + \varepsilon), \tag{65}$$

where $\varepsilon = m/c$ is assumed to be small compared with unity. The centre of the circle is displaced from the origin to $(-m, 0)$, so that the circle passes through one of the critical points of the Joukowski transformation, $\zeta = c$, which gives rise to the cusp of the airfoil in the z-plane.

In the ζ-plane, a generic point (r, θ) on the circle satisfies

$$(c + m)^2 = r^2 + m^2 + 2rm\,\cos\theta, \tag{66}$$

which leads to

$$r = -m\cos\theta + \sqrt{c^2 + 2cm + m^2\cos^2\theta}. \tag{67}$$

The airfoil surface is then given by

$$z = re^{i\theta} + \frac{c^2}{r}e^{-i\theta}, \tag{68}$$

or

$$x = \left(r + \frac{c^2}{r}\right)\cos\theta, \quad y = \left(r - \frac{c^2}{r}\right)\sin\theta. \tag{69}$$

The complex potential for a uniform flow past a circle with circulation is

$$f(\zeta) = U_0\left[(\zeta + m)e^{-i\beta} + \frac{a^2}{\zeta + m}e^{i\beta}\right] + \frac{i\Gamma}{2\pi}\log\left(\frac{\zeta + m}{a}\right). \tag{70}$$

Equation (70) along with the inverse Joukowski transformation

$$\zeta = \tfrac{1}{2}z \pm \sqrt{\frac{1}{4}z^2 - c^2} \tag{71}$$

gives the potential for the flow past an airfoil in the z-plane. The Kutta condition requires the circulation to be

$$\Gamma = 4\pi U_0 a \sin\beta. \tag{72}$$

The dissipation calculation will be carried out in dimensionless form. We choose U_0 and c to be the scales for velocity and length, respectively. The dimensionless form of the potential is

$$\frac{f(\zeta)}{U_0 c} = (\zeta + \varepsilon)\mathrm{e}^{-\mathrm{i}\beta} + \frac{(1+\varepsilon)^2}{\zeta + \varepsilon}\mathrm{e}^{\mathrm{i}\beta} + 2\mathrm{i}\sin\beta(1+\varepsilon)\log\left(\frac{\zeta+\varepsilon}{1+\varepsilon}\right). \tag{73}$$

Note that we use the same symbols for the dimensional and dimensionless variables. The inverse Joukowski transformation in the dimensionless form is

$$\zeta = \tfrac{1}{2}z \pm \sqrt{\frac{1}{4}z^2 - 1}. \tag{74}$$

The velocities can be evaluated on the potential

$$u = \frac{1}{2}\left(\frac{\mathrm{d}f}{\mathrm{d}z} + \frac{\mathrm{d}\bar{f}}{\mathrm{d}\bar{z}}\right), \quad v = \frac{\mathrm{i}}{2}\left(\frac{\mathrm{d}f}{\mathrm{d}z} - \frac{\mathrm{d}\bar{f}}{\mathrm{d}\bar{z}}\right), \tag{75}$$

and the rate of strain tensor is

$$2\boldsymbol{D} = \begin{bmatrix} \dfrac{\mathrm{d}^2 f}{\mathrm{d}z^2} + \dfrac{\mathrm{d}^2 \bar{f}}{\mathrm{d}\bar{z}^2} & \mathrm{i}\left(\dfrac{\mathrm{d}^2 f}{\mathrm{d}z^2} - \dfrac{\mathrm{d}^2 \bar{f}}{\mathrm{d}\bar{z}^2}\right) \\ \mathrm{i}\left(\dfrac{\mathrm{d}^2 f}{\mathrm{d}z^2} - \dfrac{\mathrm{d}^2 \bar{f}}{\mathrm{d}\bar{z}^2}\right) & -\left(\dfrac{\mathrm{d}^2 f}{\mathrm{d}z^2} + \dfrac{\mathrm{d}^2 \bar{f}}{\mathrm{d}\bar{z}^2}\right) \end{bmatrix}. \tag{76}$$

The surface of the airfoil is given by

$$x = \left(r + \frac{1}{r}\right)\cos\theta, \qquad y = \left(r - \frac{1}{r}\right)\sin\theta, \tag{77}$$

where

$$r = -\varepsilon\cos\theta + \sqrt{1 + 2\varepsilon + \varepsilon^2\cos^2\theta}. \tag{78}$$

Let $\dot{x} = \mathrm{d}x/\mathrm{d}\theta$ and $\dot{y} = \mathrm{d}y/\mathrm{d}\theta$, then the norm on the surface can be written as

$$\boldsymbol{n} = n_x\boldsymbol{e}_x + n_y\boldsymbol{e}_y = \frac{-\dot{y}\boldsymbol{e}_x + \dot{x}\boldsymbol{e}_y}{\sqrt{\dot{x}^2 + \dot{y}^2}}, \tag{79}$$

and

$$\mathrm{d}s = \sqrt{\dot{x}^2 + \dot{y}^2}\,\mathrm{d}\theta. \tag{80}$$

Now we calculate the dissipation

$$\mathscr{D} = \mu U_0^2 \int_A \boldsymbol{u}\cdot 2\boldsymbol{D}\cdot\boldsymbol{n}\,\mathrm{d}A = \mu U_0^2 I, \tag{81}$$

where

$$I = \int_0^{2\pi} [n_x(2\boldsymbol{D})_{xx}u + n_x(2\boldsymbol{D})_{xy}v + n_y(2\boldsymbol{D})_{yx}u + n_y(2\boldsymbol{D})_{yy}v]\sqrt{\dot{x}^2 + \dot{y}^2}\,\mathrm{d}\theta. \tag{82}$$

β	$\varepsilon=0.3$	$\varepsilon=0.2$	$\varepsilon=0.1$	$\varepsilon=0.05$	$\varepsilon=0.01$
0	4.34	3.48	2.53	2.05	1.67
$\pi/20$	6.24	6.30	9.39	22.7	410
$\pi/10$	11.8	14.5	29.3	82.8	1.59×10^3
$\pi/6$	23.7	32.3	72.6	213	4.17×10^3
$\pi/4$	43.2	61.1	142	424	8.34×10^3

TABLE 4. The integral I as a function of the attack angle β and the nose sharpness parameter ε (the smaller ε, the sharper the nose). The drag coefficient can be obtained by $C_D=-I/(2Re')$, where the Reynolds number $Re'=\rho U_0 c/\mu$. Here $c\approx l/4$, where l is the length of the airfoil.

The integral I is computed numerically. The additional drag is then obtained $D=\mathscr{D}/(-U_0)$ and the drag coefficient

$$C_D=\frac{D}{\frac{1}{2}\rho U_0^2 4c}=-\frac{\mu U_0 I}{\frac{1}{2}\rho U_0^2 4c}=-\frac{1}{Re'}\frac{I}{2}, \tag{83}$$

where the Reynolds number is

$$Re'=\frac{\rho U_0 c}{\mu}. \tag{84}$$

The drag coefficient depends on the parameter ε and the angle of attack β. The parameter ε determines the maximum thickness of the airfoil and the roundness of the leading nose. The smaller ε, the thinner the airfoil and the sharper the leading nose. In table 4, we present the magnitude of the drag coefficient multiplied by the Reynolds number as a function of the parameter ε and the angle of attack β. When ε is fixed, the magnitude of the drag coefficient increases with β. The reason is that when β is not zero, the stream must turn around the leading nose and a large amount of dissipation is generated near the leading nose. When β is fixed at zero, the dissipation decreases as ε decreases. This is because a slimmer airfoil leads to less disturbance to the uniform flow and smaller dissipation. At the limit when ε is zero, the flow becomes a uniform flow past a flat plate at a zero attack angle, in which the drag is zero. However, when β is fixed at non-zero values, the magnitude of the drag coefficient increases as ε decreases. The reason is that the major contribution to the dissipation is from the flow which turns around the leading nose. A smaller value of ε leads to a sharper leading nose and larger dissipation. At the limit when ε is zero, the leading edge coincides with one of the critical points of the Joukowski transformation, the velocity at the leading edge is singular and the dissipation calculation breaks down.

If the Reynolds number is of the order of hundreds or thousands, the additional drag is negligible when $\beta=0$ or when β is small and the airfoil is not very sharp at the leading edge; the additional drag is evident when β is non-zero and the airfoil has a very sharp leading edge.

5. Discussion and conclusion

This work concerns the drag on a body moving at a constant velocity $U_0\boldsymbol{e}_\mathrm{i}$ in an otherwise quiescent viscous liquid. The Reynolds number is high and the flow can be approximated by an outer potential flow and a boundary layer adjacent to the surface of the body. The drag is defined as

$$D=\int_A \boldsymbol{e}_\mathrm{i}\cdot\boldsymbol{T}\cdot(-\boldsymbol{n})\,\mathrm{d}A. \tag{85}$$

The dissipation calculation is one of the methods to compute the drag and it is based on the mechanical energy equation:

$$\frac{\mathrm{d}}{\mathrm{d}t}\int_V \frac{\rho|\boldsymbol{u}|^2}{2}\,\mathrm{d}V = \int_A \boldsymbol{u}\cdot\boldsymbol{T}\cdot\boldsymbol{n}\,\mathrm{d}A - \int_V 2\mu\boldsymbol{D}:\boldsymbol{D}\,\mathrm{d}V. \tag{86}$$

At steady state, (86) becomes

$$\int_A \boldsymbol{u}\cdot\boldsymbol{T}\cdot\boldsymbol{n}\,\mathrm{d}A = \int_A [\boldsymbol{u}\cdot\boldsymbol{n}(-p+\tau_n) + \boldsymbol{u}\cdot\boldsymbol{t}\tau_s]\,\mathrm{d}A = \mathscr{D}. \tag{87}$$

If the body is a gas of negligible density and viscosity, the shear stress τ_s is zero at the interface. The continuity of the normal velocity at the gas–liquid interface gives $\boldsymbol{u}\cdot\boldsymbol{n} = U_0\boldsymbol{e}_\mathrm{i}\cdot\boldsymbol{n}$. Thus, (87) can be written as

$$\int_A U_0\boldsymbol{e}_i\cdot\boldsymbol{T}\cdot\boldsymbol{n}(-p+\tau_n)\,\mathrm{d}A = \mathscr{D} \;\Rightarrow\; U_0(-D) = \mathscr{D} = \mathscr{D}_{BL} + \mathscr{D}_P, \tag{88}$$

where $\mathscr{D}_{BL}$ is the dissipation inside the boundary layer and $\mathscr{D}_P$ is the dissipation of the outer potential flow. In gas–liquid flows, the boundary layer is assumed to be very weak and $\mathscr{D}_{BL}$ is negligible to the first-order approximation. Thus, we have the drag on a gas body

$$D \approx \mathscr{D}_P/(-U_0), \tag{89}$$

which is used in our calculation of the drag on a circular gas bubble in § 2.

If the body is solid, the no-slip condition at the wall gives $\boldsymbol{u} = U_0\boldsymbol{e}_\mathrm{i}$. Thus, (87) can be written as

$$\int_A U_0\boldsymbol{e}_\mathrm{i}\cdot\boldsymbol{T}\cdot\boldsymbol{n}\,\mathrm{d}A = \mathscr{D}_{BL} + \mathscr{D}_P \;\Rightarrow\; U_0(-D) = \mathscr{D}_{BL} + \mathscr{D}_P. \tag{90}$$

The boundary layer near a solid wall is usually strong and accounts for the major part of the total dissipation. However, $\mathscr{D}_P$ is not zero and does contribute to the drag. We call $\mathscr{D}_P/U_0$ an additional drag and it is computed for an airfoil in § 4. The dissipation of the outer potential flow increases the drag calculated from the boundary-layer flow alone. Our calculation shows that the coefficient of the additional drag is proportional to $1/Re$. Thus, the additional drag is small when the Reynolds number is high.

The situation is different for a rotating cylinder moving in a liquid. The no-slip condition at the wall gives $\boldsymbol{u} = U_0\boldsymbol{e}_\mathrm{i} + \Omega a\boldsymbol{e}_\theta$, where Ω is the angular speed of the cylinder. Equation (87) can be written as

$$\begin{aligned}\int_A (U_0\boldsymbol{e}_\mathrm{i} + \Omega a\boldsymbol{e}_\theta)\cdot\boldsymbol{T}\cdot\boldsymbol{n}\,\mathrm{d}A &= U_0\int_A \boldsymbol{e}_\mathrm{i}\cdot\boldsymbol{T}\cdot\boldsymbol{n}\,\mathrm{d}A + \Omega\int_A a\tau_{\theta n}\,\mathrm{d}A,\\ &\Rightarrow U_0(-D) + \Omega T = \mathscr{D}.\end{aligned} \tag{91}$$

Equation (91) is not enough to determine two unknowns, the drag D and the torque T. Thus, the dissipation method alone cannot give the drag or the torque in this case.

Padrino & Joseph (2006) numerically simulated the flow past a rapidly rotating cylinder. When the Reynolds number is $Re = 400$ and the ratio between the cylinder rotating speed and the streaming flow speed $q/U_0 = 4$, they obtained $\mathscr{D}_{BL}:\mathscr{D}_P = 1.72{:}1$. Although in this case the dissipation cannot be used to compute the drag or the torque independently, the data show that the viscous dissipation of the outer potential flow can be significant.

In the classical boundary-layer theory of Prandtl, the viscous effect of the outer potential flow is not in evidence. The pressure across the boundary layer is assumed to

be a constant so that the irrotational pressure is imposed on the wall; in the boundary conditions at the outer edge, velocity continuity or smooth transition conditions are usually imposed and viscous stresses of the outer flow are not considered. Joseph & Wang (2004) proposed the method of VCVPF to compute a viscous correction of the irrotational pressure. VCVPF was originally derived in gas–liquid flows, in which the shear stress is zero at the interface, $\mathscr{D}_{BL}$ is negligible, and the power of the pressure correction is equal to the power of the non-zero irrotational shear stress. We applied the method of VCVPF to a circular gas bubble and obtained a drag which is the same as the result of the dissipation calculation.

We extend the idea of the viscous pressure correction from gas–liquid flows to Prandtl's boundary layer outside a solid. At the outer edge of the boundary layer, the shear stress evaluated on the boundary-layer solution using Prandtl's theory does not necessarily equal the shear stress evaluated on the outside potential flow; this is analogous to the discrepancy between the zero shear stress and non-zero irrotational shear stress at a gas–liquid interface. The shear stress discrepancy at the outer edge of the boundary layer induces extra vorticity and a viscous pressure correction. The power of the pressure correction is equal to the power of this shear stress discrepancy.

We apply the method of VCVPF to the boundary layer around a rapidly rotating cylinder in a uniform flow in § 3. The pressure correction is expanded as a Fourier series and we determine the coefficient for the $\cos\theta$ term, which is the only term in the Fourier series contributing to the drag. We integrate the pressure correction and viscous stresses to obtain the additional drag at the outer edge of the boundary layer, which is not obtained by the dissipation calculation for this problem. Numerical simulations of Padrino & Joseph (2006) confirm that the pressure in the region near the cylinder surface gives rise to a noticeable drag. After choosing an effective boundary-layer thickness, we are able to fit the pressure drag computed from VCVPF theory to the pressure drag from numerical simulation. We note that this pressure drag at the outer edge of the boundary layer is different from the pressure drag on the cylinder. Actually, the simulations of Padrino & Joseph show that the pressure drag changes sign across the boundary layer. The method of VCVPF can only determine the pressure correction at the outer edge of the boundary layer, not the variation inside the boundary layer.

Wang & Joseph (2006) carried out a new boundary-layer analysis for the flow past a rapidly rotating cylinder. They imposed the continuity of the shear stress at the outer edge of the boundary layer and solved for the pressure inside the boundary layer. The analysis shows that the pressure correction exists at the outer edge of the boundary layer and varies inside the boundary layer.

In this work, we try to understand the viscous effects of the outer potential flow on Prandtl's boundary layer. For a body moving with a constant velocity in an otherwise quiescent liquid, the non-zero viscous dissipation of the outer potential flow gives rise to an additional drag, increasing the drag calculated from the boundary-layer flow alone. The discrepancy of the shear stress at the outer edge of the boundary layer induces a viscous pressure correction of the irrotational pressure. The pressure correction varies inside the boundary layer and has viscous effects on the body, which are not captured in Prandtl's boundary-layer theory. These viscous effects of the outer flow on Prandtl's boundary layer are small when the Reynolds number is high.

This work was supported in part by the NSF under grants from Chemical Transport Systems.

REFERENCES

Ackeret, J. 1952 Über exakte Lösungen der Stokes–Navier–Gleichungen inkompressibler Flüssigkeiten bei veränderten Grenzbedingungen. *Z. Angew. Math. Phys.* **3**, 259–270.

Glauert, M. B. 1957 The flow past a rapidly rotating circular cylinder. *Proc. R. Soc. Lond.* A **242**, 108–115.

Joseph, D. D. 2003 Viscous potential flow. *J. Fluid Mech.* **479**, 191–197.

Joseph, D. D. & Wang, J. 2004 The dissipation approximation and viscous potential flow. *J. Fluid Mech.* **505**, 365–377.

Kang, I. S. & Leal, L. G. 1988*a* The drag coefficient for a spherical bubble in a uniform streaming flow. *Phys. Fluids* **31**, 233–237.

Kang, I. S. & Leal, L. G. 1988*b* Small-amplitude perturbations of shape for a nearly spherical bubble in an inviscid straining flow (steady shapes and oscillatory motion). *J. Fluid Mech.* **187**, 231–266.

Lamb, H. 1932 *Hydrodynamics*, 6th edn. Cambridge University Press (Reprinted by Dover 1945).

Levich, V. G. 1949 The motion of bubbles at high Reynolds numbers. *Zh. Eksperim. Teor. Fiz.* **19**, 18.

Maslen, S. H. 1963 Second-order effects in laminar boundary layers. *AIAA J.* **1**, 33–40.

Moore, D. W. 1959 The rise of a gas bubble in a viscous liquid. *J. Fluid Mech.* **6**, 113–130.

Moore, D. W. 1963 The boundary layer on a spherical gas bubble. *J. Fluid Mech.* **16**, 161–176.

Padrino, J. C. & Joseph, D. D. 2006 Numerical study of the steady state uniform flow past a rotating cylinder. *J. Fluid Mech.* **557**, 191–223.

Reid, E. G. 1924 *Tech. Notes Natl Adv. Comm. Aero., Washington*, no. 209.

Schlichting, H. 1960 *Boundary layer theory*, 4th edn. (trans. J. Kestin). McGraw–Hill.

Van Dyke, M. 1962 Higher approximations in boundary-layer theory. Part 1. General analysis. *J. Fluid Mech.* **14**, 161–177.

Van Dyke, M. 1969 Higher-order boundary-layer theory. *Annu. Rev. Fluid Mech.* **1**, 265–292.

Wang, J. & Joseph, D. D. 2006 Boundary-layer analysis for effects of viscosity of the irrotational flow on the flow induced by a rapidly rotating cylinder in a uniform stream. *J. Fluid Mech.* **557**, 167–190.

Wang, J., Joseph, D. D. & Funada, T. 2005 Pressure corrections for potential flow analysis of capillary instability of viscous fluids. *J. Fluid Mech.* **522**, 383–394.